SUPPORTING INFORMATION

Increased molecular conductance in oligo[*n*]phenylene wires by thermally

Woojung Lee[†], Shayan Louie[†], Austin M. Evans[†], Nicholas M. Orchanian[†], Ilana B. Stone[†],
Boyuan Zhang[‡], Yujing Wei[†], Xavier Roy[†], Colin Nuckolls*[,†], and Latha Venkataraman*[,†,‡]
[†]*Department of Chemistry and* [‡]*Department of Applied Physics and Applied Mathematics,*
Columbia University, New York, New York 10027, United States

Contents:

1. Synthesis and Characterization of OP[*n*]

OP[*2*] was purchased from Sigma Aldrich and was used without further purification.

Synthesis of OP[*3*]

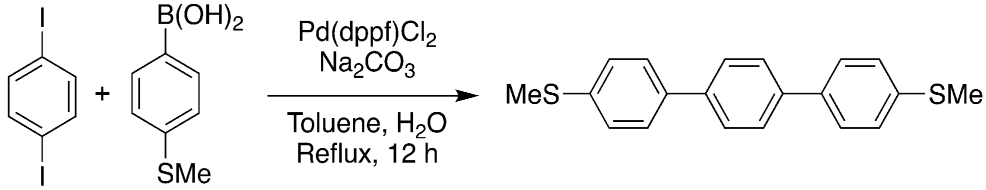

The synthesis of OP[*3*] was achieved with a modified reported procedure.[1] A 3-neck reaction flask under N_2 atmosphere was charged with 1.0 g (5.95 mmol) 4-(methylthio)phenylboronic acid, 785 mg (2.38 mmol) diiodobenzene, 1.26 g (11.9 mmol) sodium carbonate, and 9 mg (0.01 mmol) [1,1′-bis(diphenylphosphino)ferrocene]dichloropalladium(II). The solids were degassed under vacuum and the flask was refilled with N_2. In a separate flask was added 12 mL toluene and 2 mL DI water, and these were sparged with N_2. The solvents were transferred to the 3-neck reaction flask *via* cannula transfer and the mixture was heated to 100 °C for 1 hour. The temperature was then reduced to 95 °C and the solution was refluxed overnight. After cooling to room temperature, excess methanol was added, resulting in the formation of a light-yellow precipitate. This was filtered, washed with copious methanol, acetone, and dichloromethane then collected as a white powder which was dried *in vacuo*. This was further purified by silica gel column chromatography using n-hexane:DCM (1:1) prior to STM-BJ measurements.

Yield: 88% (700 mg, 2.11 mmol).
^{1}H NMR (500 MHz, $CDCl_3$, ppm): δ 7.64 (s, 4H), 7.57 (d, J=8.5 Hz, 4H), 7.35 (d, J=8.5 Hz, 4H), 2.54 (s, 6H).
^{13}C NMR (500 MHz, $CDCl_3$, ppm): δ 139.4, 137.8, 137.5, 127.3, 127.2, 127.0, 15.9.
High-Res MS (ESI+): calculated m/z for [M]+ 322.0850, found 322.0849.
IR (ATR) [cm^{-1}]: 2917, 1904, 1592, 1477, 1332, 1257, 974, 801.

Synthesis of OP[*4*]

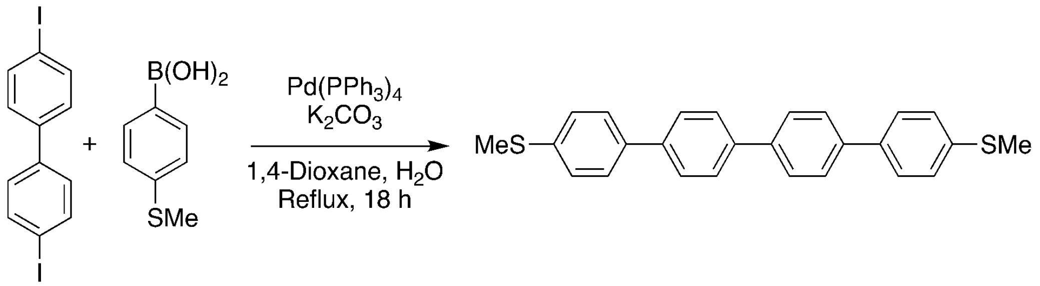

A 100 mL three-necked round bottom flask fitted with a reflux condenser and equipped with a Teflon coated stir bar under N_2 atmosphere was charged with 4,4'-diiodobiphenyl (243 mg, 0.6 mmol), (4-thiomethoxyphenyl)boronic acid (242 mg, 1.44 mmol), K_2CO_3 (414 mg, 3 mmol), and $Pd(PPh_3)_4$ (42 mg, 0.04 mmol). A separate 50 mL round bottom flask equipped with a Teflon stir bar under N_2 atmosphere was charged with 1,4-Dioxane (12 mL) and water (2.5 mL) and sparged with N_2 for 20 min. The solution was then added to the mixture of solids resulting in a bright yellow cloudy solution. The reaction mixture was refluxed for 18 h. After cooling to room temperature the solution was filtered, and the resulting beige solid was washed with DCM, MeOH and acetone.

Yield: 200 mg, 84%.
High-Res MS (ASAP+): calculated m/z for [M+H]+ 399.1241, found 399.1239.
IR (ATR) [cm^{-1}]: 3036, 3983, 2917, 2850, 1904, 1593, 1479, 1415, 1256, 1098, 1012, 975, 802.
^1H NMR (500 MHz, $CDCl_3$, ppm): δ 7.85-7.58 (m, 12H), 7.42-7.32 (m, 4H), 2.57 (s, 6H).

Synthesis of OP[5]

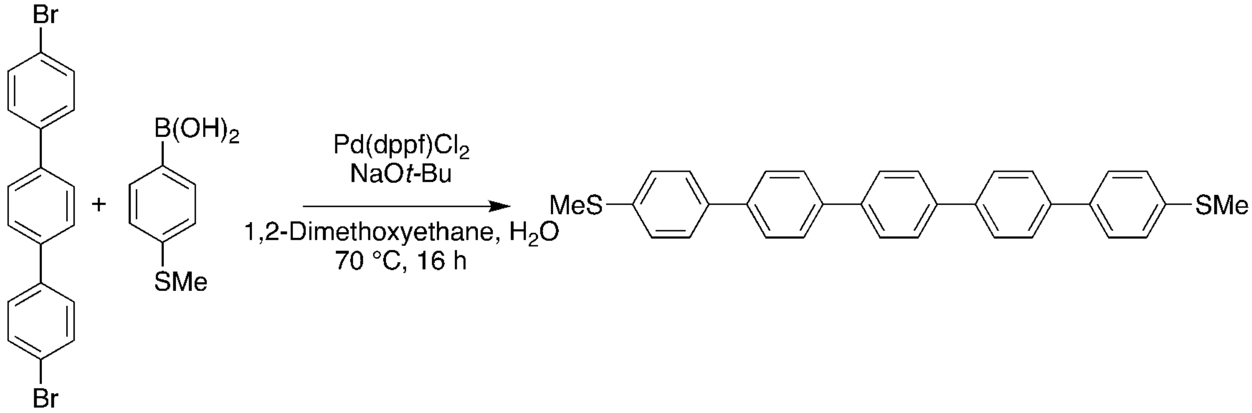

A 250 mL round bottom flask equipped with a Teflon coated stir bar under N_2 atmosphere was charged with 4,4"-dibromo-p-terphenyl (500 mg, 1.29 mmol), (4-thiomethoxyphenyl)boronic acid (541 mg, 3.22 mmol), NaO*t*-Bu (372 mg, 3.87 mmol), and $Pd(dppf)Cl_2$ (47 mg, 0.06 mmol). A separate 250 mL round bottom flask equipped with a Teflon stir bar under N_2 atmosphere was charged with 1,2-Dimethoxyethane (100 mL) and water (10 mL) and sparged with N_2 for 20 min. The solution was then added to the mixture of solids resulting in a dark brown cloudy solution. The solution was sparged again for another 20 min. The reaction mixture was stirred at 70 °C for 16 h. After cooling to room temperature the solution was filtered, and the resulting brown solid was washed with 200 mL acetone, followed by 200 mL DCM to yield an off-white powder.

Yield: 400 mg, 65%.
IR (ATR) [cm^{-1}]: 2919, 1904, 1591, 1435, 1397, 1477, 1257, 1153, 1098, 1077, 999, 803.

^{1}H NMR: An aromatic multiplet and alkyl multiplet consistent with expected NMR for OP[5] was observed using a cryoprobe on an Ascend 500 collected over ~2000 scans. Higher quality spectra were precluded by the poor solubility of OP[5]. This is consistent with previous reports which did not report proton NMR due to solubility.[2]

2. STM-BJ measurements method

The conductance of molecular wires was determined using a variable-temperature scanning tunneling microscope-break junction (STM-BJ). A gold tip and a gold-coated substrate were used as the two electrodes. As a piezo actuator is used to drive the tip in and out of contact with the substrate at a rate of 20 nm·s^{-1}. The voltage (V) and current (I) across the junction are continuously recorded at an acquisition rate of 40 kHz, and the conductance $G(= I/V)$ is calculated from these measured data. In order to exclude conductance changes due to changes in solution concentration, we measured the conductance at the higher temperature first and then at 296K without adding additional solvent or solution. Furthermore, all measurements were made at temperatures well below the solvent boiling points.

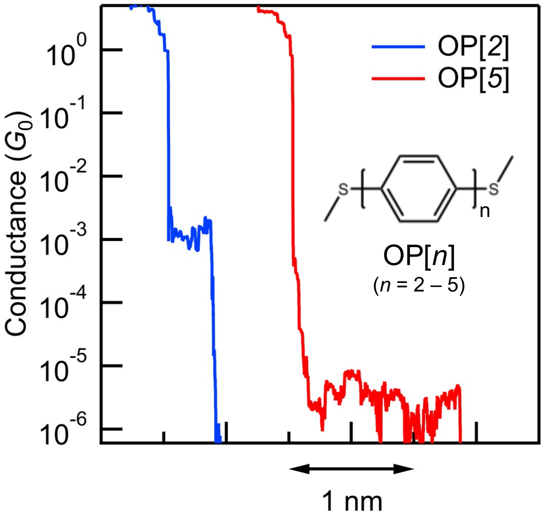

Figure S1. Sample single traces for single-molecule junctions formed from OP[*2*] (blue) and OP[*5*] (red) in TCB at 450 mV and 296 K. As expected, we find that the plateau length corresponds with the length of molecular wires.

3. Experimental data measured in octylbenezene (OB)

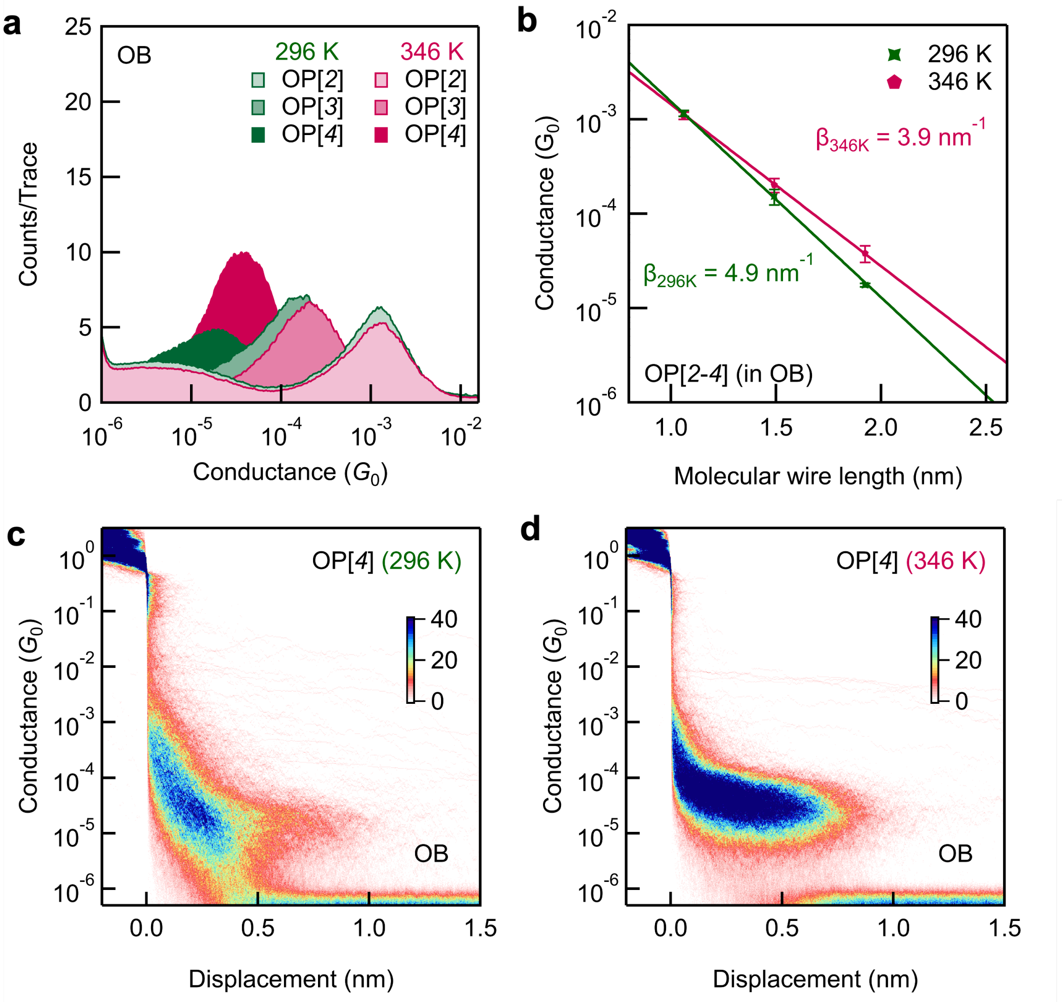

Figure S2. (a) 1D conductance histograms of OP[*2-4*] measured at different temperatures in OB. (b) Plot of conductance as a function of length for the molecules OP[*2-4*] in OB. The conductance values are fit with an exponential ($G \sim e^{-\beta L}$) to determine the decay constants (β) at each temperature. The error bars represent the standard deviation from 2-8 of independent measurements for each molecular wire. (c,d) Two-dimensional (2D) conductance-displacement histograms of OP[*4*] at two different temperatures in OB.

Table S1. The most probable conductance (G) determined by fitting a Gaussian function to the 1D histogram peaks and numerical values of conductance shift (G_{HighT} / G_{LowT}) from the experiment. The low temperature is 296 K for both solvents and high temperatures are 328 K for TCB and 346 K for OB. The longest molecular wire, OP[*5*], is not sufficiently soluble in OB.

	OP[*2*]		OP[*3*]		OP[*4*]		OP[*5*]	
Solvent	TCB	OB	TCB	OB	TCB	OB	TCB	OB
G_{LowT} (G_0)	1.26×10^{-3}	1.16×10^{-3}	2.25×10^{-4}	1.52×10^{-4}	3.04×10^{-5}	1.75×10^{-5}	4.56×10^{-6}	*
G_{HighT} (G_0)	1.28×10^{-3}	1.10×10^{-3}	2.78×10^{-4}	2.02×10^{-4}	4.99×10^{-5}	3.81×10^{-5}	9.96×10^{-6}	*
G_{HighT} / G_{LowT}	**1.01**	**0.95**	**1.24**	**1.53**	**1.64**	**2.18**	**2.18**	*

4. Total tunneling probability (P)

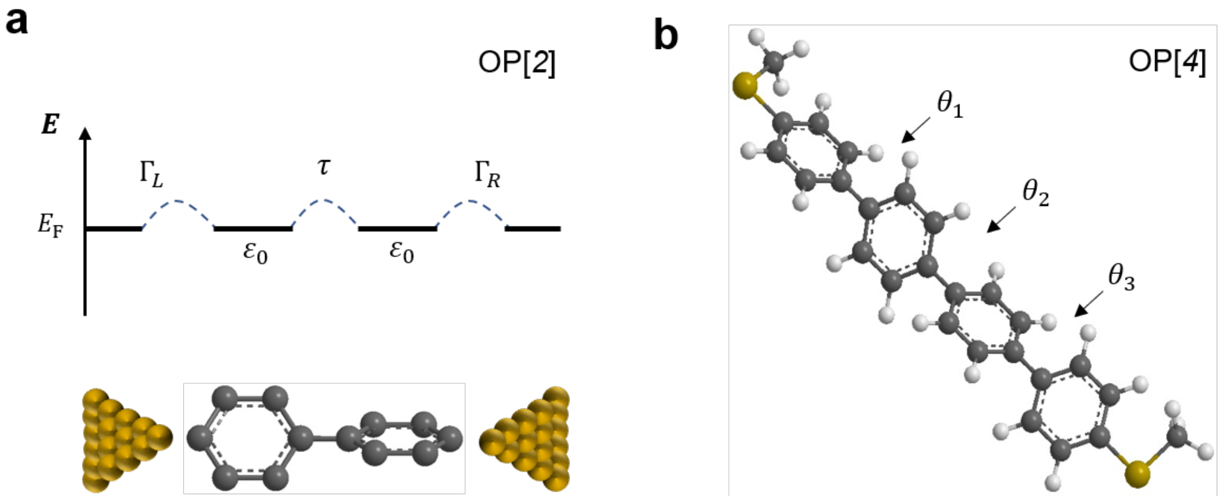

Figure S3. (a) The scheme of the simple tight-binding model where each phenyl ring of OP[*2*] has an on-site energy of ε_0 and the energy states of electrodes are filled up to the Fermi energy (E_F). Two phenyl rings are coupled by τ, and the couplings between each phenyl and electrodes have the same self-energies of $\Gamma_{L/R}$. (b) The molecular structure of OP[*4*].

According to the Landauer formalism, the total conductance can be described as the total contribution of transmission.

$$G = \frac{2e^2}{h} \sum_{n=1}^{N} T_n \tag{S1}$$

where n denotes the channel index and T_n are their individual transmissions.[3] Assuming single-channel transport, the conductance is directly proportional to transmission. To understand transmission within the molecular wires, we employ a simple tight-binding model of OP[2] without thiomethyl groups in **Figure S3a**.[3, 4] We assume that two phenyl rings have the same on-site energy (ε_0). The couplings between the electrode (left or right) and the terminal phenyl are expressed as $\Gamma_{L/R}$, different from the coupling between adjacent phenyl rings, τ.[3]

In our model system, the Hamiltonian of the isolated molecular wire, H_{wire}, and the Green's function matrix, $G(E)$, can be written as[3, 5]

$$H_{wire} = \begin{bmatrix} \varepsilon_0 & \tau \\ \tau & \varepsilon_0 \end{bmatrix} \tag{S2}$$

$$G(E) = [E - H_{wire} - \Sigma_L - \Sigma_R]^{-1} \tag{S3}$$

$$= \begin{bmatrix} E - \varepsilon_0 - i\Gamma_L & -\tau \\ -\tau & E - \varepsilon_0 - i\Gamma_R \end{bmatrix}^{-1}$$

where E is the energy of the transmitted electron and $\Sigma_{L/R}$ are the self-energies matrices. Assuming the OP[*2*] is symmetric and two phenyl rings have identical couplings with electrodes, ($\Gamma_L = \Gamma_R = \Gamma$) we can derive the expression of transmission in an off-resonant tunneling regime as[3, 6]

$$T(E) = \frac{4\Gamma^2}{|E-\varepsilon_0|^4}|\tau|^2 \tag{S4}$$

Eq. S4 can be expanded for OP[*2-5*][3] as

$$T(E) = \frac{4\Gamma^2}{|E-\varepsilon_0|^{2n}}|\tau|^{2(n-1)} = \frac{4\Gamma^2}{|E-\varepsilon_0|^{2n}}|\tau_1|^2|\tau_2^2| \cdots = \tag{S5}$$

where n is the number of phenyl rings and τ_i is the coupling between the i^{th} and $i^{th}+1$ phenyl. In other word, each dihedral coupling (τ_i) has an impact of τ_i^2 on transmission independently. Since the inter-phenyl coupling depends on the overlap of the π-orbitals of the adjacent phenyls, τ has a cosine-squared relation with the inter-ring dihedral angle, as shown in the main paper.

We empirically derived the independence relation of rotational barriers (ε) within each molecular wire of oligo[n]phenylenes along dihedral angles,

$$\varepsilon(\theta_1, \theta_2, \cdots, \theta_j) \approx \varepsilon(\theta_1) + \varepsilon(\theta_2) + \cdots + \varepsilon(\theta_j) \tag{S6}$$

where j (= n - 1) is the total number of dihedral couplings. With the fact that each dihedral coupling has an independent impact on total transmission, we can expect that tunneling probability at a dihedral site, $\mathrm{P}(\theta_i)$, is proportional to τ_i^2 ($\propto cos^2\theta_i$) and the probability of reaching a certain θ_i ($e^{\frac{-\varepsilon(\theta)}{kT}}$),

$$\mathrm{P}(\theta_i) \propto cos^2\theta_i \cdot e^{\frac{-\varepsilon(\theta_i)}{kT}} \tag{S7}$$

Therefore, total tunneling probability within OP[n] can be calculated by multiplying all tunneling probabilities of each pivot point within the molecular wire, as shown in eq. 3,

$$\mathrm{P}(\theta_1, \cdots, \theta_j) \sim \prod_{i=1}^{j} cos^2\theta_i \cdot e^{-\frac{\varepsilon(\theta_i)}{kT}} .$$

5. Average tunneling probability ($\overline{\mathrm{P}}$)

We can consider $\mathrm{P}(\theta_1)$, $\mathrm{P}(\theta_2)$, ···, $\mathrm{P}(\theta_j)$ as ($1 \times \alpha$) matrices respectively, where j is the number of pivot points, and α is the number of available dihedral angles at each pivot point. Considering eq. 3, the total tunneling probability, $\mathrm{P}(\theta_1, \cdots, \theta_j)$, is an j-dimensional matrix, representing available tunneling probability combinations among all pivot points. We sum all elements of this *j*-dimensional matrix in order to obtain the integral of the tunneling probabilities for all configurations. Also, by dividing the integral by α^j, we find the average tunneling probabilities ($\overline{P}$) at all available angle sets. As $P(\theta_1,\cdots,\theta_j) \leq 1$, the theoretical maximum integral of tunneling probabilities is α^j. For the OP[*n*] system, we can calculate the average tunneling probability as,

$$\overline{P} = \frac{\sum P(\theta_1,\cdots,\theta_j)}{\alpha^j} \tag{S8}$$

Table S2. Average tunneling probabilities ($\overline{P}$) at all dihedral angles and the numerical values of tunneling probability shift ($\overline{P}_{328K}$ / $\overline{P}_{296K}$). Tunneling probability is calculated at low temperature (296 K) and high temperatures (328 K and 346 K) for OP[*2-5*].

	OP[*2*]	OP[*3*]	OP[*4*]	OP[*5*]
$\overline{P}_{296K}$	2.10×10^{-1}	4.43×10^{-2}	8.87×10^{-3}	1.67×10^{-3}
$\overline{P}_{328K}$	2.22×10^{-1}	4.96×10^{-2}	1.05×10^{-2}	2.10×10^{-3}
$\overline{P}_{346K}$	2.28×10^{-1}	5.23×10^{-2}	1.14×10^{-2}	2.37×10^{-3}
$\overline{P}_{328K}$ / $\overline{P}_{296K}$	**1.06**	**1.12**	**1.18**	**1.26**
$\overline{P}_{346K}$ / $\overline{P}_{296K}$	**1.09**	**1.18**	**1.29**	**1.42**

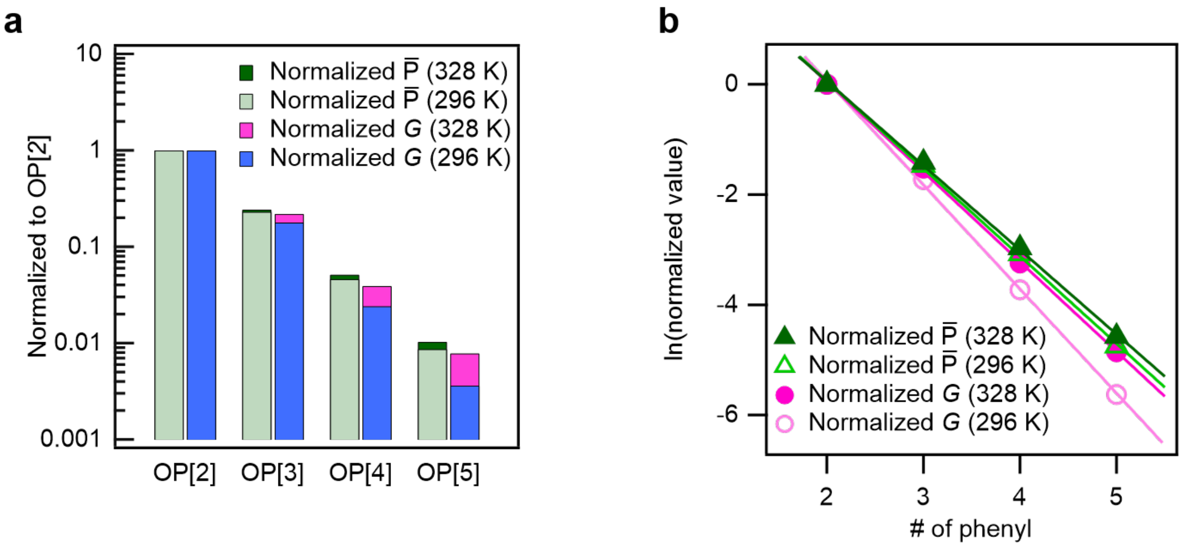

Figure S4. (a) Average tunneling probabilities ($\overline{P}$) of OP[*n*] are normalized to $\overline{P}$ of OP[*2*], and the measured conductance (*G*) is normalized to *G* of OP[*2*] at two different temperatures. (b) The normalized $\overline{P}$ and *G* decrease as the molecular wire length increases, and the trends are well fitted to exponential function.

To more thoroughly investigate the relation between tunneling probability and the experimentally measured conductance, we normalized each value to those of OP[*2*] at the two different temperatures in **Figure S4a**. Although the trends agree very well, our tight-binding model is clearly a bit too simple to obtain a quantitative agreement with the experiment (**Figure S4b**).

6. Impact of thermal broadening on Fermi distribution of the leads

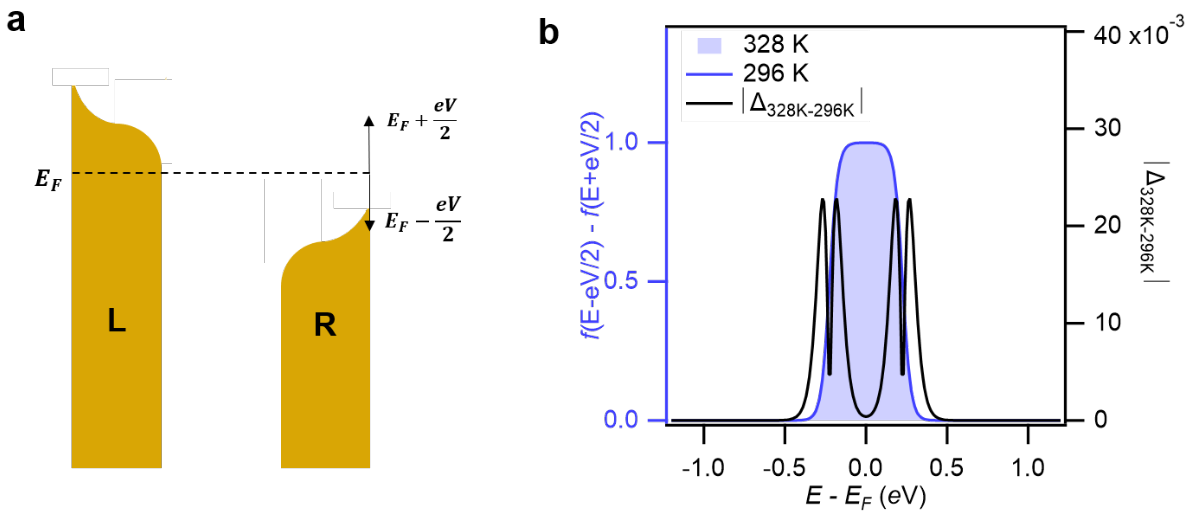

Figure S5. (a) The energy diagram of tunneling junction between two gold electrodes where E_F is the Fermi level, V is the applied bias, and e is the electron charge. (b) The Fermi-Dirac distribution between two electrodes at two different temperatures (296 K and 346 K) and the difference value ($|\Delta_{328K-296K}|$) between Fermi-Dirac distributions at two different temperatures. The applied bias (V) is 450 mV.

Within the Landauer approach, the total current across the junction (**Figure S5a**) can be expressed as

$$I(V) = \frac{2e}{h}\int_{-\infty}^{\infty} dE\, T(E)\left[f\left(E-\frac{eV}{2}\right) - f\left(E+\frac{eV}{2}\right)\right] \tag{S9}$$

where $T(E)$ is the energy dependent transmission function, $f\left(E \mp \frac{eV}{2}\right)$ is the Fermi-Dirac distribution of the electron reservoir. The Fermi-Dirac is:

$$f(E) = \frac{1}{e^{E/kT}+1} \tag{S10}$$

where E is the energy, k is the Boltzmann constant, and T is the temperature. The calculated Fermi-Dirac distribution between two electrodes and the difference between these at 328K and 296K are shown in **Figure S5b** for an applied voltage V = 450 mV.

We also computed electronic transmission through oligo[n]phenylene using a non-equilibrium Green's function formalism implemented within the AITRANSS package.[7, 8] (**Figure S6a**) This density functional theory (DFT) based calculations were carried out using closed-shell Kohn-Sham formulation with FHI-aims software.[9] The Kohn-Sham states were represented in an optimized all-electron numeric atom-centered basis set with "light" computational settings. We used the PBE exchange-correlation functional[10], and scalar relativistic corrections to the kinetic energy were included in the first-principles calculations at the atomic zeroth-order regular approximation (ZORA) level.[11] Using eq. S9, we obtain the current as a function of voltage, $I(V)$, as shown in **Figure S6b**. As expected by examing the difference in the Fermi-Dirac distribution at the two experimental temperatures, the $I(V)$ function has no discernable temperature dependence. Using $G = I/V$, we calculate conductance the experimental bias of 450 mV. The theoretically determined conductance is temperature independent. (**Table S3**) These results solidify our main result by demonstrating that thermally enhanced planarization is the main reason for the conductance increase.

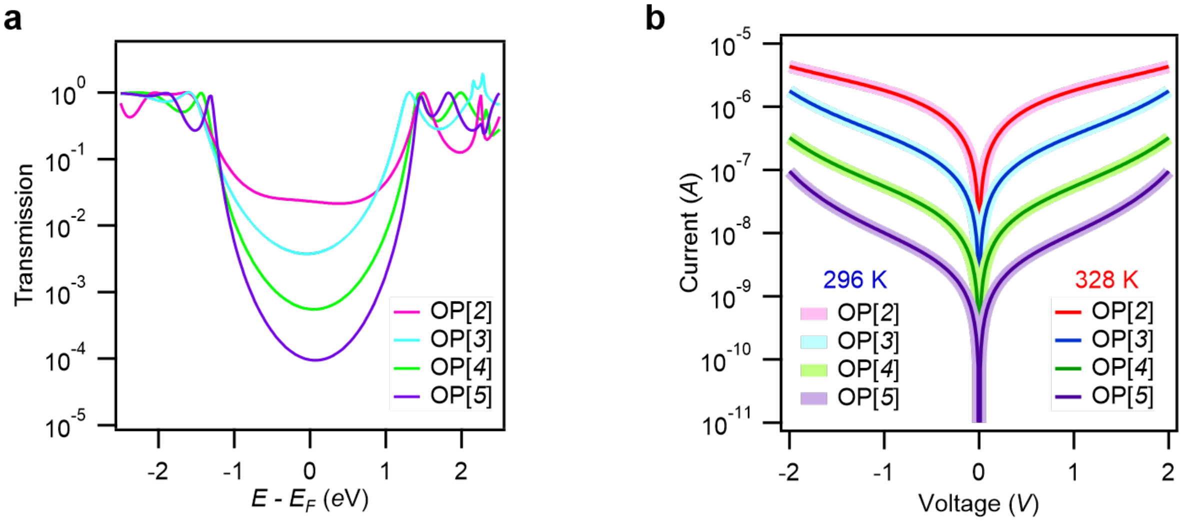

Figure S6. (a) Au-molecule-Au junction transmission function of OP[*2-5*]. (b) Calculated current-voltage relation at two different temperatures from Landauer formula.

Table S3. Calculated conductance (G) at 450 mV, and the numerical values of temperature dependence on conductance.

	OP[*2*]	OP[*3*]	OP[*4*]	OP[*5*]
G_{296K} (G_0)	2.32×10^{-2}	3.92×10^{-3}	5.83×10^{-4}	1.02×10^{-4}
G_{328K} (G_0)	2.32×10^{-2}	3.93×10^{-3}	5.83×10^{-4}	1.02×10^{-4}
G_{296K} / G_{296K}	**1.00**	**1.00**	**1.00**	**1.00**

References

(1) Joseph, Y.; Peić, A.; Chen, X.; Michl, J.; Vossmeyer, T.; Yasuda, A., Vapor sensitivity of networked gold nanoparticle chemiresistors: importance of flexibility and resistivity of the interlinkage, *J. Phys. Chem. C,* **2007,** 111, 12855-12859.
(2) Shved, A. M.; Nelyubina, Y. V.; Perekalin, D. S., Synthesis of cyclopentadienyl iron complexes with substituted phenylene ligands via Suzuki coupling, *J. Orgomet. Chem.,* **2020,** 906, 121061.
(3) Cuevas, J. C.; Scheer, E., *Molecular electronics: an introduction to theory and experiment.* World Scientific: Hackensack, NJ, 2010.
(4) Tsuji, Y.; Movassagh, R.; Datta, S.; Hoffmann, R., Exponential attenuation of through-bond transmission in a polyene: Theory and potential realizations, *ACS Nano,* **2015,** 9, 11109-11120.

(5) Gunasekaran, S.; Greenwald, J. E.; Venkataraman, L., Visualizing quantum interference in molecular junctions, *Nano Lett.,* **2020,** 20, 2843-2848.
(6) Datta, S., *Electronic transport in mesoscopic systems*. Cambridge university press: 1997.
(7) Arnold, A.; Weigend, F.; Evers, F., Quantum chemistry calculations for molecules coupled to reservoirs: Formalism, implementation, and application to benzenedithiol, *J. Chem. Phys.,* **2007,** 126, 174101.
(8) Bagrets, A., Spin-polarized electron transport across metal–organic molecules: A density functional theory approach, *J. Chem. The. Comp.,* **2013,** 9, 2801-2815.
(9) Blum, V.; Gehrke, R.; Hanke, F.; Havu, P.; Havu, V.; Ren, X.; Reuter, K.; Scheffler, M., Ab initio molecular simulations with numeric atom-centered orbitals, *Comp. Phys. Comm.,* **2009,** 180, 2175-2196.
(10) Perdew, J. P.; Burke, K.; Ernzerhof, M., Generalized gradient approximation made simple, *Physical review letters,* **1996,** 77, 3865.
(11) Lenthe, E. v.; Baerends, E.-J.; Snijders, J. G., Relativistic regular two-component Hamiltonians, *J. Chem. Phys.,* **1993,** 99, 4597-4610.